AGU PUBLICATIONS

JGR

Journal of Geophysical Research: Atmospheres

RESEARCH ARTICLE
10.1002/2017JD027431

Key Points:
- New features in the updraft-limited regime improve the understanding of the height dependency of aerosol-cloud interaction regimes
- Particle equilibrium super saturation plays an important role in understanding the new features of the updraft-limited regime
- A new parameterization is proposed for the dependence of rain initiation height on aerosol number concentration and vertical velocity

Supporting Information:
- Supporting information S1
- Data Set S1
- Data Set S2
- Data Set S3
- Data Set S4
- Data Set S5
- Data Set S6

Correspondence to:
J. Chen,
jingyi.chen@stonybrook.edu

Citation:
Chen, J., Liu, Y., Zhang, M., & Peng, Y. (2018). Height dependency of aerosol-cloud interaction regimes. *Journal of Geophysical Research: Atmospheres*, *123*, 491–506. https://doi.org/10.1002/2017JD027431

Received 10 JUL 2017
Accepted 8 DEC 2017
Accepted article online 18 DEC 2017
Published online 10 JAN 2018

Height Dependency of Aerosol-Cloud Interaction Regimes

Jingyi Chen[1], Yangang Liu[1,2], Minghua Zhang[1,3], and Yiran Peng[4]

[1]School of Marine and Atmospheric Sciences, Stony Brook University, Stony Brook, NY, USA, [2]Brookhaven National Laboratory, Upton, NY, USA, [3]ICCES/Institute of Atmospheric Physics, Chinese Academy of Sciences, Beijing, China, [4]Ministry of Education Key Laboratory for Earth System Modeling and Department of Earth System Science, Tsinghua University, Beijing, China

Abstract This study investigates the height dependency of aerosol-cloud interaction regimes in terms of the joint dependence of the key cloud microphysical properties (e.g., cloud droplet number concentration and cloud droplet relative dispersion) on aerosol number concentration (N_a) and vertical velocity (w). The three distinct regimes with different microphysical features are the aerosol-limited regime, the updraft-limited regime, and the transitional regime. The results reveal two new phenomena in updraft-limited regime: (1) the "condensational broadening" of cloud droplet size distribution in contrast to the well-known "condensational narrowing" in the aerosol-limited regime and (2) above the level of maximum supersaturation; some cloud droplets are deactivated into interstitial aerosols in the updraft-limited regime, whereas all droplets remain activated in the aerosol-limited regime. Further analysis shows that the particle equilibrium supersaturation plays important role in understanding these unique features. Also examined is the height of warm rain initiation and its dependence on N_a and w. The rain initiation height is found to depend primarily on either N_a or w or both in different N_a-w regimes, suggesting a strong regime dependence of the second aerosol indirect effect.

1. Introduction

Aerosols influence weather and climate through directly scattering and absorbing radiation (termed as the direct aerosol effect) and indirectly serving as cloud condensation nuclei (CCN) and ice nuclei (termed as the indirect aerosol effect) (Albrecht, 1989; Haywood & Boucher, 2000; Lohmann & Feichter, 2005; Twomey, 1974, 1977). Twomey (1974, 1977) pointed out that an increase in aerosol number concentration (N_a) leads to increases in CCN and cloud droplet number concentration (N_c), which in turn reduces droplet sizes and enhances cloud albedo when liquid water remains unchanged. Although the notion of N_c increasing with increasing N_a is well understood qualitatively, and several parameterizations have been developed (hereafter number effect; see Ghan et al., 2011, for a recent review), the so-called aerosol indirect effects remain among the most uncertain climate forcings according to the latest Intergovernmental Panel on Climate Change report (Intergovernmental Panel on Climate Change, 2013). Furthermore, climate models tend to overestimate the cooling of aerosol indirect effects and are more susceptible to aerosols compared to observations (Lohmann & Lesins, 2002; Ruckstuhl et al., 2010). Reducing model uncertainty and reconciling models with observations continue to be a major challenge facing the climate science community after decades of research.

Two microphysical factors have been proposed to be partially responsible for the tenacious problem. The first is the regime dependence of N_c on N_a. It is well known that for a given updraft velocity (w), the dependence of N_c on N_a is nonlinear and regime-dependent: N_c increases linearly with N_a when N_a is low, but the N_c-N_a relationship becomes sublinear when N_a is high (Feingold et al., 2001). Reutter et al. (2009) classified the nonlinear N_c-N_a relationship into three distinct regimes using a detailed cloud parcel model: (1) the aerosol-limited regime is characterized by high w/N_a ($\geq 10^{-3}$ m s^{-1} cm^3), high parcel supersaturation (S_p), and strong (linear) dependence of N_c on N_a but weak dependence of N_c on w; (2) the updraft-limited regime is characterized by low w/N_a ($\leq 10^{-4}$ m s^{-1} cm^3), low S_p, and weak dependence of N_c on N_a but strong dependence of N_c on w; and (3) the transitional regime falls between the aerosol-limited and updraft-limited regimes with sublinear dependence of N_c on both N_a and w. They also suggested further studies in the less emphasized updraft-limited regime with more aerosols.

The second microphysical factor is the dispersion effect whereby changes in aerosol properties alter the spectral shape of the cloud droplet size distribution in addition to droplet number concentration. Liu and Daum

(2002) showed, by analyzing data from marine clouds under a variety of aerosol conditions with N_c ranging from tens to a few hundred, that increased N_a leads to concurrent increases of N_c and cloud droplet relative dispersion (ε) (i.e., the ratio of cloud droplet standard deviation to cloud droplet mean radius), and the enhanced ε negates the number effect and may be partly responsible for the overestimated indirect aerosol effect and the discrepancy between model estimates of the indirect aerosol effect and those constrained by observations (Kumar et al., 2016; Peng & Lohmann, 2003; Penner et al., 2006; Rotstayn & Liu, 2003, 2009). This finding of ε increasing with N_a is consistent with some subsequent observational studies (Chen et al., 2012; Lu et al., 2007; Pandithurai et al., 2012; Peng & Lohmann, 2003), parcel model simulations (Ching et al., 2012, 2016; Peng et al., 2007; Wood et al., 2002; Yum & Hudson, 2005), and theoretical analysis (Liu et al., 2006). On the other hand, several studies (Berg et al., 2011; Hudson et al., 2012; Lu et al., 2012; Ma et al., 2010; Martins & Dias, 2009) reported conflicting observations of decreasing ε with increasing N_a. It is noteworthy that the studies reporting decrease of ε with increasing N_a are mainly in clouds affected by heavy pollution (e.g., several thousand aerosols per cc and several hundred of mean N_c from Ma et al., 2010), heavy biomass burning (e.g., up to N_c = 1,284 cm^{-3} in Martins & Dias, 2009), or Amazonian clouds (e.g., N_a up to 4,093 cm^{-3} in Cecchini et al., 2017), as opposed to the increase of ε with increasing N_a being found mostly in clean marine clouds.

Chen et al. (2016) systematically examine the codependence of N_c and ε on N_a and w using an adiabatic parcel model. It was shown that given w, ε increases with increasing N_a in the aerosol-limited regime, peaks in the transitional regime, and decreases with further increasing N_a in the updraft-limited regime. This finding reconciles contrasting observations in literature and reinforces the compensating role of dispersion effect. The nonmonotonic behavior of ε further quantifies the relationship between the transitional N_a and w that separates the aerosol- and updraft-limited regimes.

However, previous aerosol-cloud interaction (ACI) studies, including ours in Chen et al. (2016), have been primarily focused on the height of maximum supersaturation (see Appendix B for details). Although N_c being a constant above the height of maximum supersaturation seems to be a reasonable assumption, it may be problematic under certain conditions, for example, higher N_a, low w, larger mode radius, and/or anthropogenically influenced aerosol type (Nenes et al., 2001).

Furthermore, it is well known that ε depends strongly on the height above cloud base (Çelik & Marwitz, 1999; Peng et al., 2007). Traditional condensational theory predicts that condensational growth leads to narrowing of cloud droplet size distribution with height (Lamb & Verlinde, 2011). Observational studies show that the variation of ε with height depends on the pollution level of the clouds (Pawlowska et al., 2006). Also, the cloud radiative effects are determined by the whole cloud layer above cloud base. Thus, the complete ACI regime is likely height-dependent. However, systematic study of the ACI regime dependence on height is still lacking, and thus, the first objective of this study is to extend Chen et al. (2016) to investigate the height dependence of the ACI regime.

The second objective of this study is to examine the dependence of rain initiation height on aerosol properties and vertical velocity. Many studies have shown that aerosol-induced precipitation suppression not only horizontally increases the cloud fraction as conceived by Albrecht (1989) and Liou & Ou (1989) but also may vertically increase the cloud top height depending on thermodynamic conditions of atmosphere (Pincus & Baker, 1994; Wood, 2007). Satellite studies have found that higher cloud tops are in polluted cumulus clouds (Yuan et al., 2011) and open cell stratocumulus clouds (Christensen & Stephens, 2011) than in clean clouds. But conflicting results have been reported. For example, Segrin et al. (2007) and Christensen and Stephens (2011) found that pollution only led to insignificant cloud top changes in close cell stratocumulus clouds. Li et al. (2011) found little changes of warm cloud tops over the U.S. Southern Great Plain with aerosols. Our systematic examination of the regime dependence of rain initiation height on N_a and w can provide physical insight into this important issue, because rain initiation and the subsequent drizzling process are some of the primary factors that determine the cloud top height and cloud fraction.

The remainder of this paper is organized as follows. Section 2 describes numerical experimental settings and calculations. Section 3 presents the results and reveals the unique features of cloud microphysical properties in aerosol- and updraft-limited regimes. Key findings are summarized and discussed in Section 4.

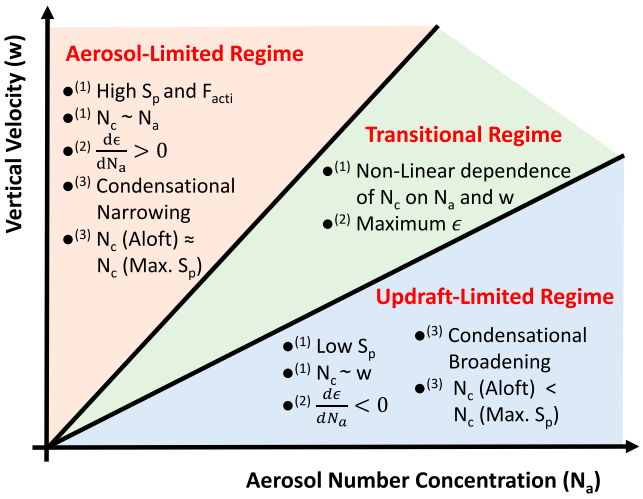

Figure 1. Schematic illustration of the main characteristics of aerosol-cloud interaction regimes. Details about the item with superscript (1), (2), and (3) are discussed in Reutter et al. (2009), Chen et al. (2016) and this paper, respectively. Note that the transitional regime defined by the ϵ behavior at the level of maximum supersaturation is a single line, i.e., for a fixed set of aerosol properties other than N_a. The region of transitional regime in this figure is used to schematically illustrate the range of aerosol properties.

2. Model and Numerical Experiments

The cloud parcel model used in this study (Chen et al., 2016) contains the full treatment of droplet nucleation and condensation following the widely used method of "Lagrangian bins" (Heymsfield & Sabin, 1989; Howell, 1949; Leaitch et al., 1986). When the parcel rises and cools, water vapor is condensed on the particles. To simplify the problem, the cloud parcel is treated as a closed system without exchange of air, particles, and energy. Entrainment-mixing, sedimentation, and collision-coalescence processes are not considered in this study (see Appendix A for detailed descriptions of the equations used in the model).

The initial aerosol size distribution is assumed to be lognormal with geometric mean radius of 0.06 μm and geometric standard deviation of 1.5 (Reutter et al., 2009). The hygroscopicity is 0.61 assuming ammonium sulfate (Petters & Kreidenweis, 2007). The effect of different initial aerosol size distributions on the results is also examined and is discussed in the supporting information. Simulations are performed with 1,000 Lagrangian particle size bins to represent the cloud droplet size distribution. Time step is $\frac{1.0m}{w}$, except between cloud base and maximum supersaturation where a shorter step ($\frac{0.1m}{w}$) is used to identify the level of maximum supersaturation more accurately. The vertical resolution of model output is 10 m from cloud base to 600 m and 100 m above 600 m; the higher resolution in the lower part of clouds facilitates detailed examination of physical processes in the early stage of droplet formation. Parallel computing (OpenMP) is used to facilitate a large number of simulations.

3. Results

3.1. Regime Dependency of Vertical Profiles

Based on Reutter et al. (2009) and Chen et al. (2016), the dependency of key cloud properties on N_a and w is classified into three different regimes at maximum supersaturation height. Figure 1 is a schematic figure summarizing the key microphysical features of each regime. The information superscripted by (1) and (2) is summarized in this paragraph based on previous studies, and the information superscripted by (3) will be discussed in detail in this paper. First, the aerosol-limited regime is characterized by low N_a/w, high S_p, high activation fraction, a strong dependence of N_c on N_a, and a positive relation between ϵ and N_a. Second, the updraft-limited regime is characterized by high N_a/w, low S_p, low activation fraction, a strong dependence of N_c on w, and a negative relation between ϵ and N_a. Third, the transitional regime is located between the aerosol-limited and updraft-limited regimes, exhibits a nonlinear dependence of N_c on N_a and w, and the largest values of ϵ are also in transitional regime. In general, the ratio of N_a to w is a good metric gauging the aerosol-cloud interaction regimes: the aerosol-limited regime, transitional regime, and updraft-limited regime correspond to $N_a/w < x$, $N_a/w = x$, and $N_a/w > x$, respectively, where $x = 5.7 \times 10^{-4}$ m s^{-1} cm^3 is estimated by curve-fitting the relationship between the transitional w and the N_a corresponding to the maximum ϵ (e.g., Figure 3 of Chen et al., 2016). Note the slight difference of this fitting coefficient from that (5.3×10^{-4} m s^{-1} cm^3) in Chen et al. (2016), which is due to the differences in the model settings (e.g., number of particle bins and time step) and air heat capacity used (dry air in Chen et al., 2016 and moist air in this study).

To investigate the height dependency, we partition the 2,500 simulations (50 values of N_a logarithmically distributed between 10 and 10^5 cm^{-3} and 50 values of w logarithmically distributed between 0.05 and 20 m s^{-1}) into six groups according to the ratio N_a/w ranging from aerosol-limited regime to updraft-limited regime. Figure 2 shows the vertical variations of mean values of S_p, N_c, and ϵ in different N_a/w groups. The dashed warm color represents aerosol-limited regime; the solid cold color represents the updraft-limited regime; the thick black line denotes the transitional regime, which is defined by the maximum ϵ for each w at the height of maximum supersaturation as shown in Chen et al. (2016). The height relative to the cloud base is

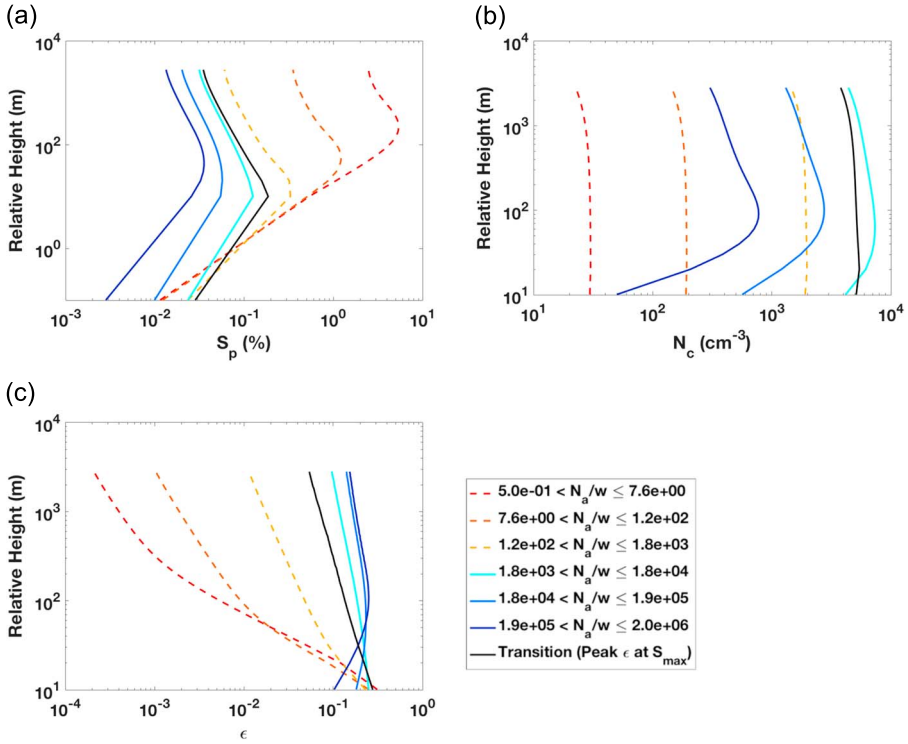

Figure 2. Vertical profiles of (a) parcel supersaturation (S_p), (b) cloud droplet number concentration (N_c), and (c) cloud droplet relative dispersion (ϵ) at different ratios of aerosol number concentration (N_a) to vertical velocity (w). The thick black line denotes the transitional regime that divides the aerosol-limited (dashed) and updraft-limited regime (solid) (see text for details). The numbers of cases in each N_a/w group are 179, 500, 722, 588, 376, and 136, respectively.

hereafter referred to as height for convenience. Note that the simulation is stopped when air temperature reaches −8°C to strictly concentrate on warm cloud processes (Crawford et al., 2012; Li, Xue, & Yang, 2013).

The profiles in Figure 2a show that S_p remains larger in the aerosol-limited regime than in the updraft-limited regime during parcel rising. It is also evident that N_c almost holds constant above the level of maximum supersaturation in the aerosol-limited regime as commonly assumed. However, in the updraft-limited regime, N_c first increases with height, peaks at a certain height above the level of maximum supersaturation, and then decreases with further increasing heights. The highest N_c occurs near the transitional regime. As will be detailed in section 3.2, such "unconventional" change of N_c with height is due to the so-called "kinetic effect" (Chuang et al., 1997; Nenes et al., 2001).

The height dependency of ε (Figure 2c) is more interesting: ϵ decreases rapidly with height above 10 m in the aerosol-limited regime but decreases much slower or even increases in the updraft-limited regime. Above 110 m, ϵ decreases with height in both regimes. To understand the behavior of Figure 2c, Figures 3a and 3b further show the cloud droplet size standard deviation (σ) and mean radius (R_{mean}) as a function of height, respectively. Figure 3a shows decreasing σ in the aerosol-limited regime but increasing σ in the updraft-limited regime. In the aerosol-limited regime, larger particles grow slower than smaller particles and the droplet size distribution narrows with height, because particle equilibrium supersaturation (S_k) is much smaller than S_p and can be ignored. In contrast, in the updraft-limited regime, larger particles grow faster than smaller particles and the size distribution broadens due to the dependence of S_k on droplet size (see appendix in Chen et al., 2016). Grabowski et al. (2011) also showed that σ increases with time at lower w in their Lagrangian simulations. The condensational narrowing in the aerosol-limited regime has been abundantly studied in the published literature and textbooks (e.g., Pruppacher & Klett, 1997); however, the condensational broadening in the updraft-limited regime has not received much attention because both S_k and the variations of S_k with droplet size are usually assumed to be small and ignored (see Appendix C for more quantitative analysis).

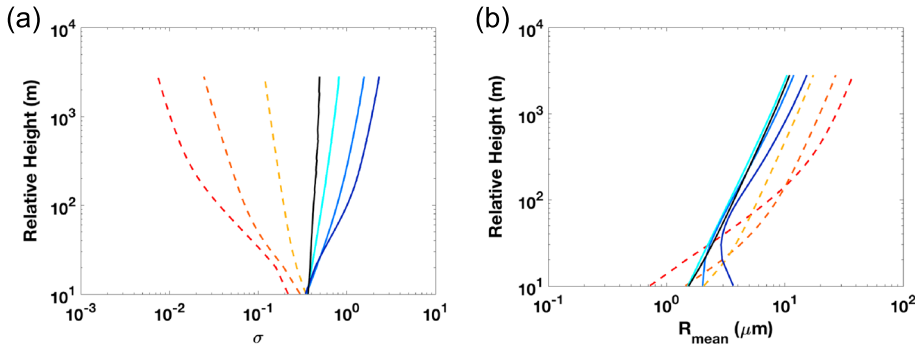

Figure 3. Same as Figure 2, except for (a) cloud droplet standard deviation (σ) and (b) cloud droplet mean radius (R_{mean}).

The increasing σ and slower growing R_{mean} (Figure 3b) lead to the slower decrease of ϵ with height in the updraft-limited regime. Based on the analysis of the data at 1,000 m height, ϵ, σ, and $\frac{1}{R_{\text{mean}}}$ in the extreme updraft-limited regime (1.9×10^5 cm^{-3} m^{-1} s $< N_a/w \leq 2.0\times10^6$ cm^{-3} m^{-1} s) are larger than the corresponding values in the extreme aerosol-limited regime (0.5 cm^{-3} m^{-1} s $< N_a/w \leq 7.6$ cm^{-3} m^{-1} s) by the factor of 448.70, 187.23, and 2.51, respectively.

To further investigate how the dependence of S_k on droplet size influences cloud properties, Figure 4 show the results from a suite of simulations, which are like those shown in Figures 2 and 3, except that the S_k of the median cloud droplet bin (e.g., the S_k of the 300th activated bin if the number of activated particle bins are 600) has applied to all the cloud droplets when solving the condensational growth equation (equations (A1a) and (A1b)) in the code. The purpose of this experiment is to dissect the effect from the dependence of S_k on droplet size. Comparison of Figures 4a and 2a shows that larger values of N_a/w correspond to larger values of the differences of S_p between Figures 4a and 2a in the updraft-limited regime, which suggests that ignoring the dependence of S_k on droplet size overestimates the S_p, especially when N_a/w is large. Comparison between Figures 4b and 2b shows that droplets do not evaporate and deactivate in the higher part of clouds when the dependence of S_k on droplet radius is ignored in the updraft-limited regime. Compared to Figure 2c, Figure 4c shows a smaller ϵ for all cases and faster decreasing at high levels in the updraft-limited regime. Figures 4d and 4e show that ignoring dependence of S_k on droplet size leads to a smaller σ for all the cases. The decreasing σ with height in the updraft-limited regime when change of S_k with radius is ignored confirms that the "condensational broadening" in the updraft-limited regime is the result of variations of S_k with particle sizes. Smaller values of R_{mean} in the updraft-limited regime in Figure 4e than those in Figure 3b are consistent with the N_c profiles (Figures 4b and 2b): more activated cloud droplets lead to smaller cloud droplet radius. Based on the analysis of the data of Figure 4 at 1,000 m, ϵ, σ, and $\frac{1}{R_{\text{mean}}}$ in the extreme updraft-limited regime are larger than the corresponding values in the extreme aerosol-limited regime by the factor of 137.47, 11.58, and 12.31, respectively. A comparison of Figures 2 and 4 indicates that the vertical profiles of ϵ are due to more σ than R_{mean} when considering the dependence of S_k on droplet size because the regime variation of σ is stronger than R_{mean}. These features suggest that dependence of S_k on droplet size causes evaporation/deactivation of small particles, and thus spectral broadening in the updraft-limited regime. Also, ε becomes 1–2 order smaller if the dependence of S_k on droplet size is neglected, which implies that S_k is critical for all cases even in the aerosol-limited regime.

To illustrate the detailed regime dependence on N_a and w at different heights, Figure 5 shows regime dependence of N_c and ε at three typical heights of 20 m (Figures 5a and 5b), 560 m (Figures 5c and 5d), and 2,110 m (Figures 5e and 5f) above cloud base. At 20 m, only some cases (1,412 out of 2,500) have reached their maximum supersaturation. At 560 m, all the cases just have reached their levels of maximum supersaturation. At 2,110 m, the variation of ϵ with height becomes stable (relative changes of the mean values in each N_a/w group are less than 3% per 100 m). Besides the similar characteristics to those at the maximum supersaturation, it is interesting to note that N_c starts to decrease with increasing N_a at the lower part of the cloud when N_a is larger than about 10^4 cm^{-3} (Figure 5a). This is because S_p decreases with

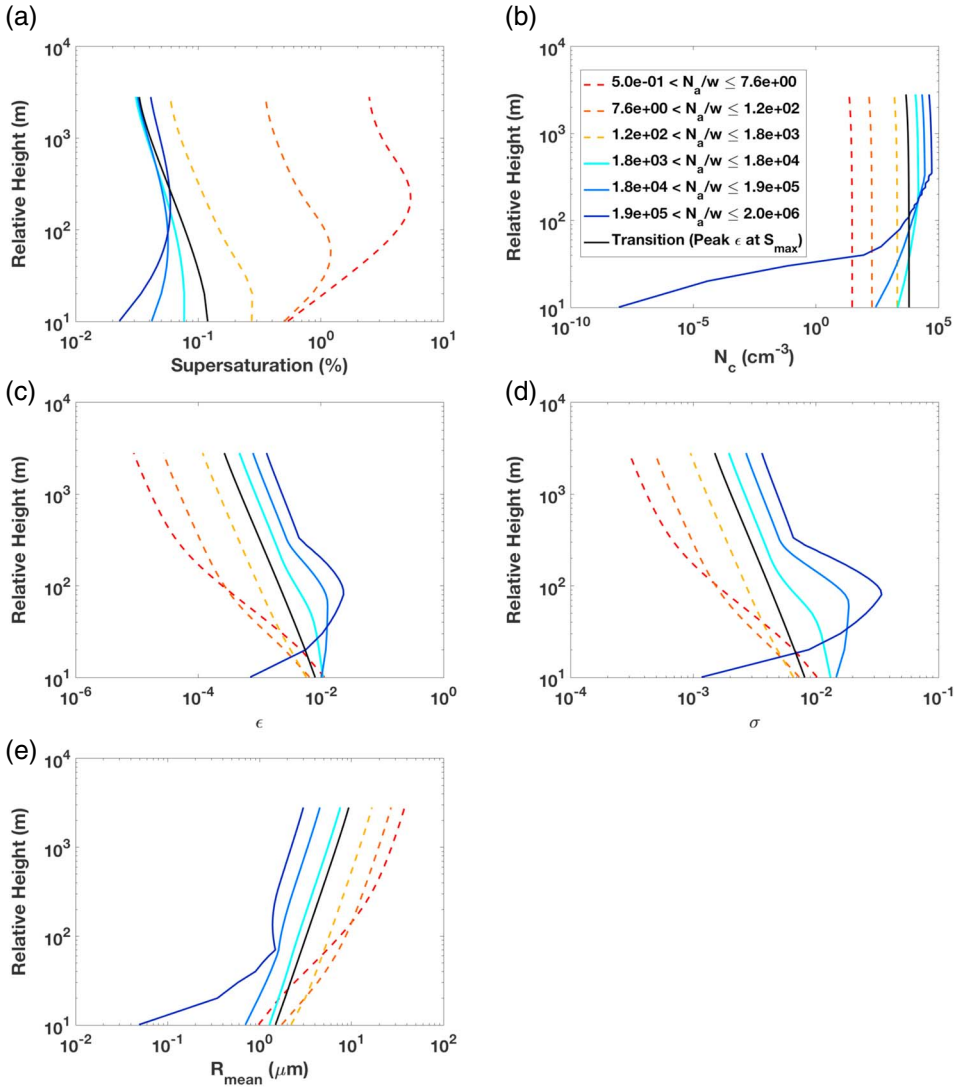

Figure 4. Vertical profiles of (a) S_p, (b) N_c, (c) ϵ, (d) σ, and (e) R_{mean} when S_k are assumed to be the same for all the cloud droplets.

increasing N_a faster just above cloud base than in higher levels. The patterns at the two other altitudes are similar to each other as shown in Figures 5c and 5e, except that N_c increases more rapidly with increasing N_a in updraft-limited regime at 560 m than at 2,110 m, which implies decreasing of N_c with height above 560 m. Figures 5b, 5d, and 5f show the dependence of ϵ on N_a and w at 20 m, 560 m, and 2,110 m, respectively. The similar pattern of regime dependence remains at different altitudes, with the peak ϵ shifting to higher N_a as the cloud parcel rises higher. After a few hundred meters above the maximum supersaturation, the branch of decreasing ϵ with increasing N_a disappears within the ranges of N_a and w examined.

Figure 6 examines σ and R_{mean} at the same levels as Figure 5. The plots of σ substantiate the spectral narrowing in the aerosol-limited regime and spectral broadening in the updraft-limited regime from 20 m to 2,110 m. For the same N_a, a larger (smaller) w corresponds to a narrower (broader) size distribution. These phenomena are consistent with Figure 3a and can be explained by the different magnitudes of S_p minus S_k in the different regimes. Plots of R_{mean} show that particle growth from 20 m to 2,110 m in the aerosol-limited regime is more prominent than those in the updraft-limited regime, which can be explained by the theory that the competition among particles for available water vapor in the updraft-limited regime is enhanced.

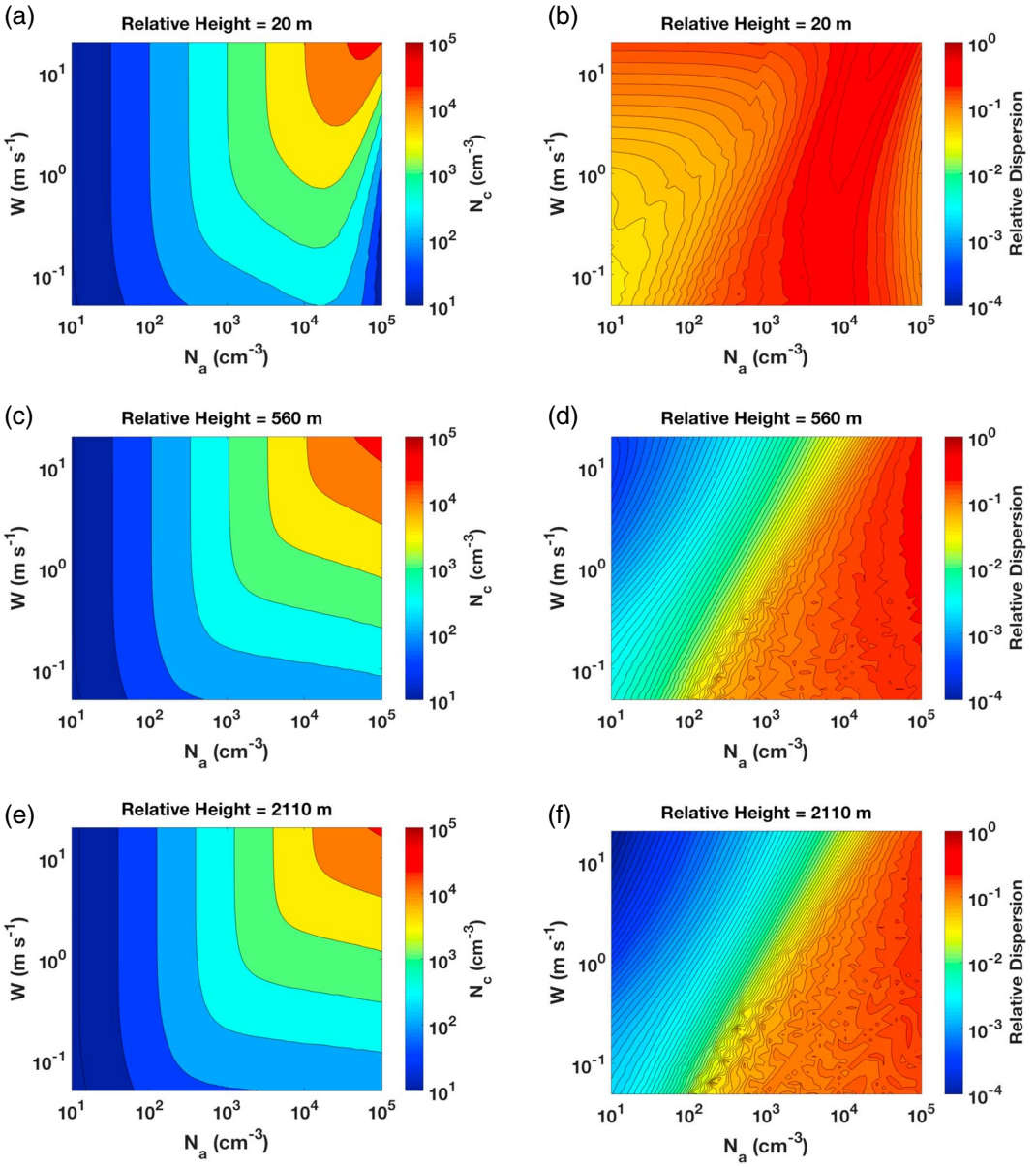

Figure 5. Joint dependence on N_a and w of (a, c, and e) cloud droplet number concentration and (b, d, and f) cloud droplet relative dispersion at 20 m (Figures 5a and 5b), 560 m (Figures 5c and 5d), and 2,110 m (Figures 5e and 5f), respectively.

3.2. "Kinetic Effects" and Their Impacts on Cloud Droplet Number Concentration

The decrease of N_c with increasing N_a above the level of maximum supersaturation in the updraft-limited regime as shown in Figure 2b is more evident in Figure 7, which shows N_c normalized by their maximum values in each regime group. The three profiles from the aerosol-limited regime converge and decrease with height due to the parcel volume expansion. The three profiles from the updraft-limited regime show that the strengths of evaporation and deactivation at higher levels depend on regimes. This section examines the physical mechanism behind this phenomenon.

Nenes et al. (2001) demonstrated three types of kinetic effects termed as "inertial mechanism," "evaporation mechanism," and "deactivation mechanism." Briefly, inertial mechanism mostly influences those particles growing from large dry aerosols. These particles always have a large critical radius, which needs sufficient time to reach, and thus, mostly, they are unable to reach their critical radius in the lower part of clouds, but their size is large enough to play important role in radiation and precipitation. Evaporation mechanism

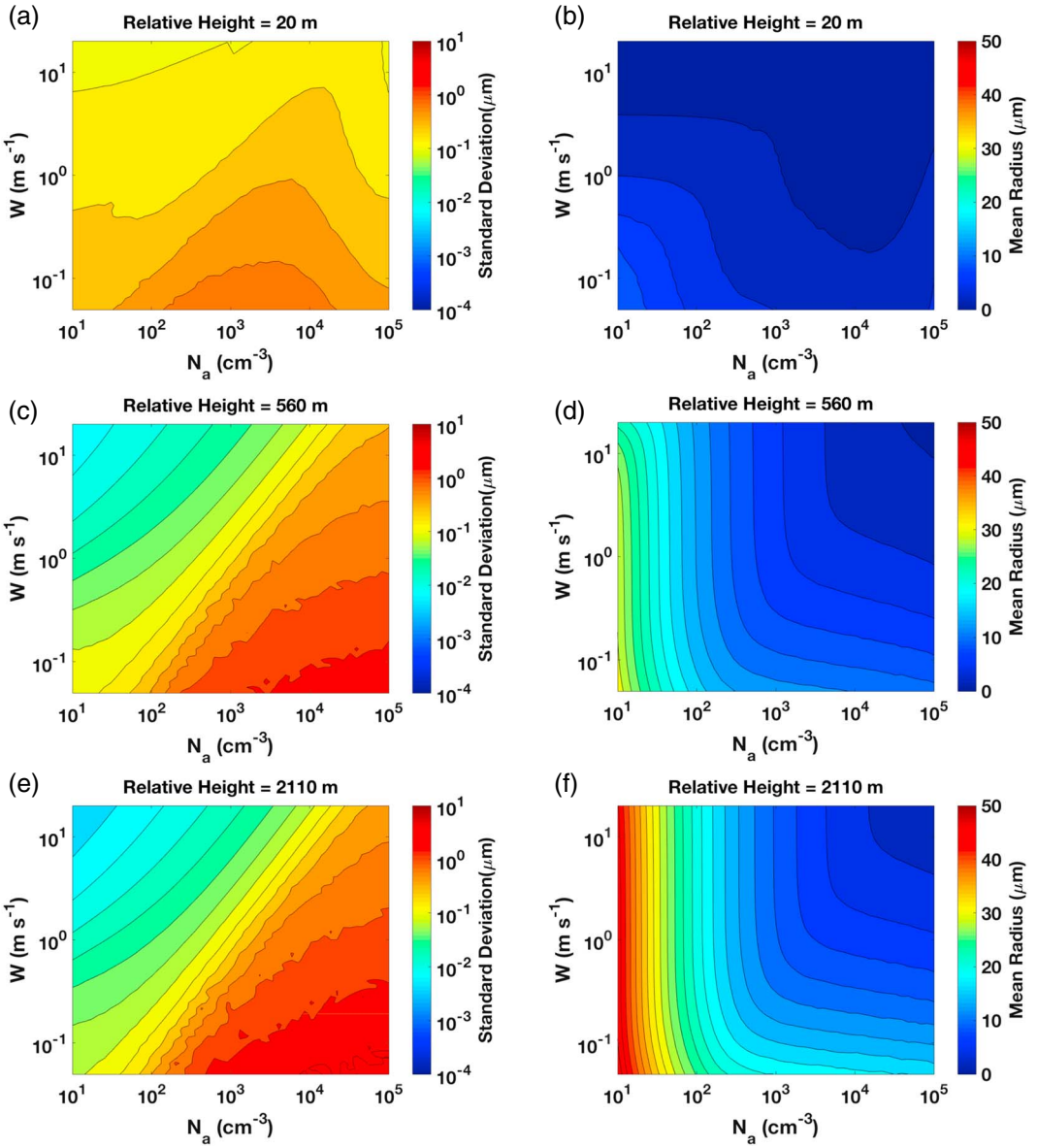

Figure 6. Regime dependency of (a, c, and e) cloud droplet standard deviation and (b, d, and f) cloud droplet mean radius on aerosol number concentration and vertical velocity at 20 m (Figures 6a and 6b), 560 m (Figures 6c and 6d), and 2,110 m (Figures 6e and 6f).

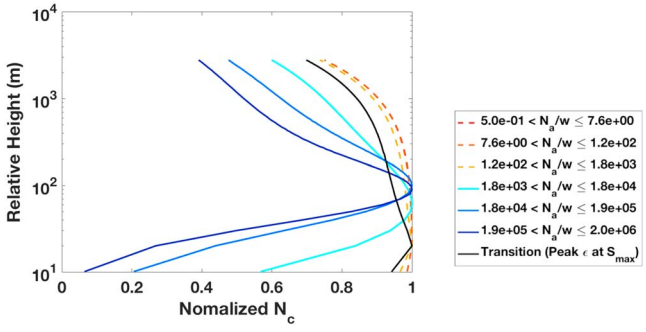

Figure 7. Vertical profiles of normalized N_c by the maximum N_c for each profile. The meanings of each color are the same as Figure 2.

applies to those particles that could be potentially activated but evaporate to form interstitial aerosols because the time they are exposed to high supersaturation is not long enough. Deactivation mechanism applies to those activated particles that evaporate into interstitial aerosols because S_p drops below S_k. The kinetic effects can be further illustrated by examining the differences between S_p and S_k that drives condensation/evaporation of particles.

Figures 8a and 8b show two examples of vertical variations of S_k and S_p at different size bins in the aerosol-limited regime and updraft-limited regime, respectively. The black lines are the particle bins with the smallest activated particles at maximum supersaturation; the green circles represent the particle bins with smallest activated particles at about

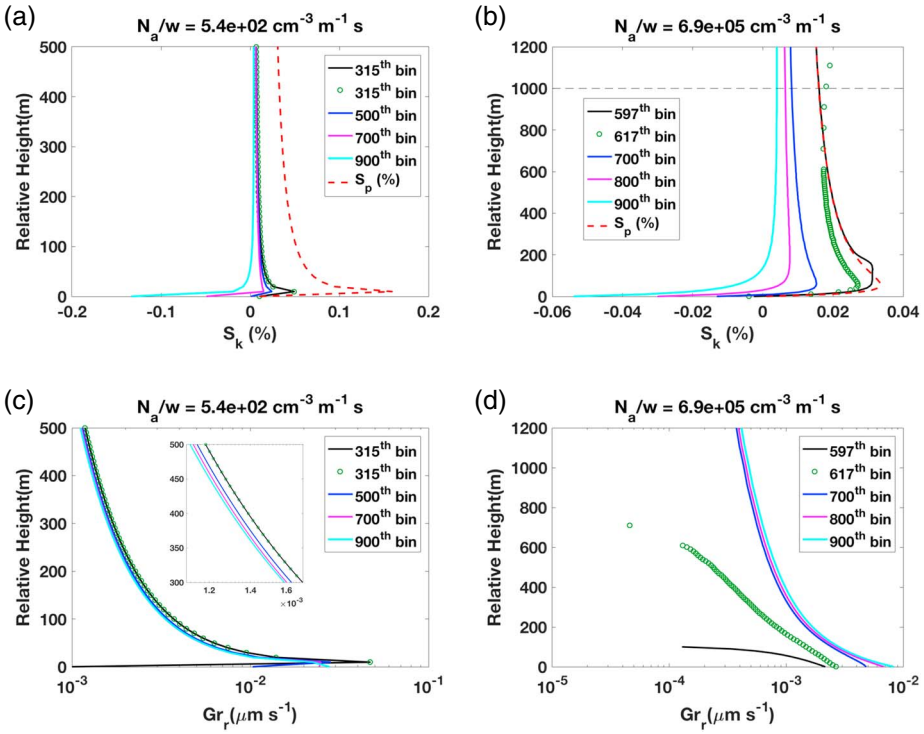

Figure 8. Typical examples of the vertical profile of (a and b) particle equilibrium supersaturation and (c and d) radius growth rate in aerosol-limited regime (Figures 8a and 8c) and updraft-limited regime (Figures 8b and 8d). The black line denotes the smallest bin activated at the maximum supersaturation. The green circles denote the smallest bin activated at 1,000 m. The red dash line denotes the parcel supersaturation. A higher bin number corresponds to a larger dry aerosol radius. The w is 0.1 m s^{-1} for both examples.

1,000 m. Initially, dry aerosols are assigned to each particle bins in the order of increasing sizes, and the same order remains when particles grow by condensation. In the typical aerosol-limited regime, S_p is much larger than S_k even when the parcel rises high; thus, the smallest activated particle at maximum supersaturation always remains activated. However, in the typical updraft-limited regime, S_p is only slightly larger than S_k near the level of maximum supersaturation. Small differences between S_p and S_k cause small "driving force" for growth. Since S_p decreases with height faster than S_k does, at 1,000 m (Figure 8b), the particles in the 597th bin evaporate and deactivate into interstitial particles, and the 617th bin becomes the smallest activated particle bin. Similarly, the 617th size bin is no longer the smallest activated particle bin when the parcel further rises higher than 1,000 m, because particles of that size bin have S_k larger than S_p, evaporate and eventually deactivate. This is the same as evaporation mechanism or deactivation mechanism identified by Nenes et al. (2001): Both evaporation mechanism and deactivation mechanism applies to the particles with their critical supersaturation lower than S_{max} but higher than local S_p. Thus, they evaporate from cloud droplets to interstitial aerosols ultimately. When local S_p becomes smaller than S_k, evaporation mechanism applies to the particles with radius smaller than the Köhler critical radius while deactivation mechanism applies to the particles with radius larger than their Köhler critical radius. Thus, deactivation mechanism is the primary reason for decreasing N_c above maximum supersaturation. Note that in this study, the definition of cloud droplets follows that given by Reutter et al. (2009): particles are larger than the critical radius $r_{c,cld}$ as equations (1a) and (1b) shown.

$$r_{c,cld} = \frac{2\,a}{3\,S_p} \tag{1a}$$

$$a = \frac{2\sigma_s}{\rho_w R_w T} \tag{1b}$$

where σ_s is surface tension, ρ_w is the water density, R_w is gas constant for water, and T is air temperature. Likewise, droplets will deactivate into particles when their radii are smaller than $r_{c,cld}$. Although $r_{c,cld}$ is not

exactly the Köhler critical radius, deactivation mechanism is still the most plausible mechanism to cause the decrease of N_c. Because decreasing S_p leads to increasing $r_{c,\mathrm{cld}}$ (equations (1a) and (1b)), the evaporated particle has their radius larger than $r_{c,\mathrm{cld}}$ but smaller than the $r_{c,\mathrm{cld}}$ at the next time step. This requires that the evaporated particle has larger S_k and hence smaller radius growth rate. Smaller dry particle size contributes to larger S_k (equations (A9a)–(A9c)). Thus, the evaporated particles are mostly the ones with their radii slightly larger than $r_{c,\mathrm{cld}}$ and with their Köhler critical radius smaller than the particle size, which corresponds to the deactivation mechanism.

Figures 8c and 8d show the radius growth rate of the same cases as Figures 8a and 8b. In the typical aerosol-limited regime, larger particles have smaller growth rate than smaller particles. While in the typical updraft-limited regime, larger particles have larger growth rate than smaller particles. Note that the differences of radius growth rate of the 700th bin and 900th bin are not significant below 200 m because the supersaturation differences "S_p-S_k" are large.

To summarize, the smaller differences between S_k and S_p in the updraft-limited regime cause loss of some small cloud droplets and thus decrease of N_c through the deactivation mechanism.

3.3. Regime Dependence of Rain Initiation Height

Rain initiation is critical for understanding warm rain processes (Beard & Ochs, 1993; Magaritz-Ronen et al., 2016; Wang & Grabowski, 2009). Recent studies investigated the rain initiation height by assuming a certain effective radius (r_e) (or volume mean radius) as an empirical threshold of rain initiation (Freud & Rosenfeld, 2012). However, systematic examination of the dependence of the rain initiation height on the N_a and w (or regime dependence of rain initiation height) is still lacking. Liu et al. (2005) derived a physically based threshold function as a function of droplet concentration, liquid water content, and relative dispersion. Liu et al. (2008) further related this threshold function to threshold radar reflectivity and reported observational evidence for the dependence of the threshold radar reflectivity on N_c. Here we take advantage of this theoretical autoconversion threshold function to examine the regime dependence of rain initiation height.

Briefly, the autoconversion threshold function (T_{auto}) (Liu et al., 2005, 2006) is given as

$$T_{\mathrm{auto}} = \frac{\int_{r_{c,\mathrm{rain}}}^{\infty}\left(\int_{r_{c,\mathrm{rain}}}^{\infty} K(r_1,r_2) r_2^3 n(r_2) dr_2\right) n(r_1) dr_1}{\int\left(\int K(r_1,r_2) r_2^3 n(r_2) dr_2\right) n(r_1) dr_1} \quad or \tag{2a}$$

$$T_{\mathrm{auto}} = \left[\frac{\int_{r_{c,\mathrm{rain}}}^{\infty} r^6 n(r) dr}{\int_0^{\infty} r^6 n(r) dr}\right]\left[\frac{\int_{r_{c,\mathrm{rain}}}^{\infty} r^3 n(r) dr}{\int_0^{\infty} r^3 n(r) dr}\right] \tag{2b}$$

$$r_{c,\mathrm{rain}} = 2.8522 \frac{N_c^{\frac{1}{6}}}{\mathrm{LWC}^{\frac{1}{3}}} \tag{2c}$$

where $K(r_1, r_2)$ is the collection kernel between droplets with radius as r_1 and r_2, r is droplet radius, $n(r)$ is the droplet size distribution, $r_{c,\mathrm{rain}}$ is the critical radius of rain initiation given by Liu et al. (2004), and LWC is the liquid water content. The threshold function T_{auto} ranges between 0 and 1 and measures the strength of collection process relative to the diffusional growth; a larger T_{auto} indicates a relatively stronger occurrence of collection process. Equations (2a)–(2c) reveal that LWC and, thus T_{auto}, increases with height as the parcel rises, eventually leading to drizzle formation or the start of collection process. In this study, $1 \geq T_{\mathrm{auto}} \geq 0.9$ is used to define the rain initiation height. Note that our sensitivity study using different values of T_{auto} (i.e., 0.1, 0.3, 0.5, 0.7, and 0.9) shows that the results reported in this study are not sensitive to the choice of T_{auto} value (not shown).

Figure 9 presents the joint dependency of rain initiation height (H_{rain}) on N_a and w (Figure 9a); also shown are the regime dependence of the corresponding LWC (Figure 9b), N_c (Figure 9c), and ϵ (Figure 9d). The blank area indicates that the air temperature is lower than −8°C and the simulation stops after T_{auto} reaches 0.9. Evidently, the basic pattern of H_{rain} is like that of N_c: H_{rain} depends primarily on N_a when N_a/w is low in the aerosol-limited regime and on w when N_a/w is high in the updraft-limited regime. The close resemblance of the corresponding LWC and H_{rain} reflects the linear relationship between LWC and height (Albrecht et al., 1990). The general pattern of N_c is same as those at other levels. Figure 9d shows that ϵ has low

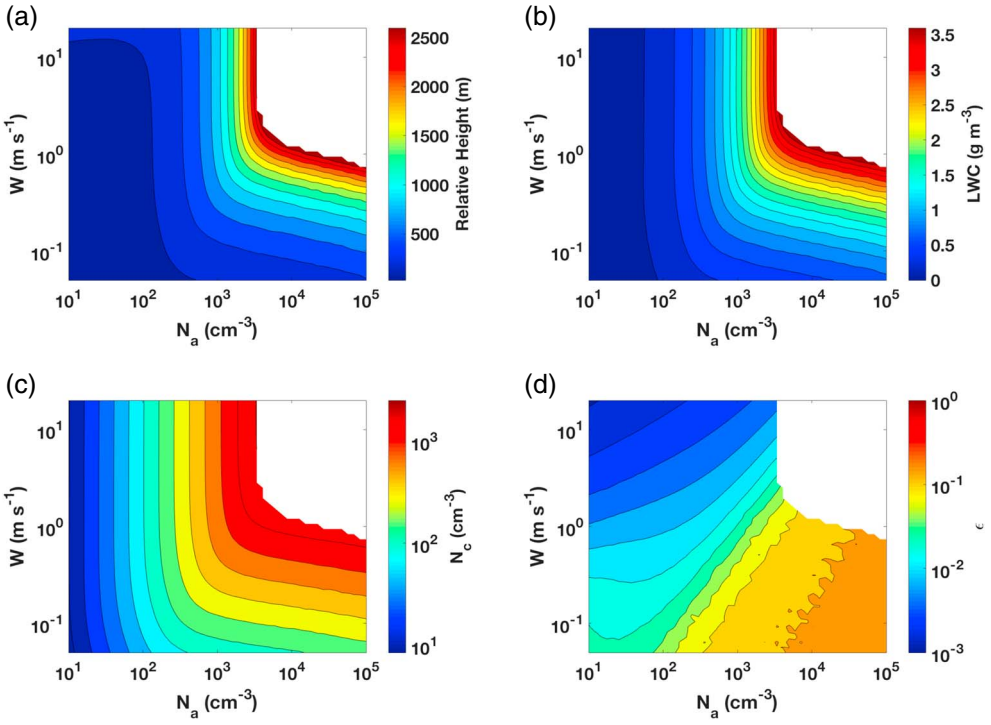

Figure 9. Joint dependency on N_a and w of (a) rain initiation height, (b) liquid water content (LWC), (c) cloud droplet number concentration, and (d) relative dispersion at the height of rain initiation.

values in the aerosol-limited regime and high values in the updraft-limited regime at H_{rain}, consistent with the condensational narrowing in the aerosol-limited regime and condensational broadening in the updraft-limited regime.

Further, it is desirable to have an analytical expression for quantifying the regime dependence of H_{rain}. We find that the relationship between H_{rain} and N_a normalized by the corresponding transitional regime values (superscripted by an asterisk) is virtually collapsed onto a single curve (Figure 10). The transitional regime values correspond to maximum relative dispersion at each w at the height of maximum supersaturation (equations (3b) and (3c)). It can be seen that H_{rain}/H_{rain}^* first increases rapidly with increasing N_a/N_a^* in the aerosol-limited regime ($N_a/N_a^* < 1$) and gradually levels off in the updraft-limited regime ($N_a/N_a^* > 1$). The "universal" curve can be described by

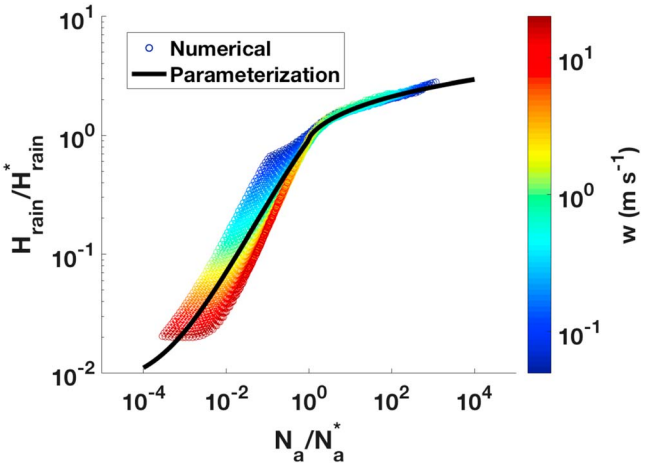

Figure 10. Relationship between the normalized height of rain initiation and the normalized aerosol based on the 2,500 simulations. The corresponding values at peak relative dispersion at maximum supersaturation are used for the normalization. The black line is the piecewise fitting given by equations (3a)–(3c).

$$\frac{H_{rain}}{H_{rain}^*} = \begin{cases} \dfrac{-3.926}{1+\exp\left(0.6339*\ln\left(\dfrac{N_a}{N_a^*}\right)-1.195\right)}+3.934 & \dfrac{N_a}{N_a^*}\le 1 \\ 0.3644*\left(\ln\left(\dfrac{N_a}{N_a^*}\right)\right)^{0.7711}+0.9398 & \dfrac{N_a}{N_a^*}>1 \end{cases} \quad (3a)$$

$$H_{rain}^* = 1.570\times10^3\, w^{0.781} \quad (3b)$$

$$N_a^* = 1.752\times10^3\, w \quad (3c)$$

where the expressions for H_{rain}^* and N_a^* are obtained by fitting the numerical simulations. The units of H_{rain}, w, and N_a are m, m s^{-1}, and cm^{-3}, respectively. To the best of our knowledge, equations (3a)–(3c) are the first expression that quantifies the codependence of rain initiation height on N_a and w.

It is worth noting that the collision coalescence process is not considered in the parcel model; some changes of the results are expected if collision coalescence process is considered in view of its role in determining the cloud droplet size distribution (Feingold et al., 1996; Wood, 2006). The effect of collision-coalescence process is expected to be larger in the aerosol-limited regime more than in updraft-limited regime because of larger R_{mean} (Figure 3b). In view of the limitations of this study (e.g., adiabatic parcel model without considering collision-coalescence process), it needs to be evaluated against more sophisticated numerical simulations such as large-eddy simulations and measurements.

4. Conclusions and Discussions

This work extends our previous study to examine the height dependence of aerosol-cloud interaction regime, especially, height dependency of N_c and ϵ as a joint function of N_a and w. Also investigated, for the first time, is the regime dependence of H_{rain} on N_a and w.

Analysis shows that cloud droplet size distributions experience spectral narrowing with height in the aerosol-limited regime, but spectral broadening with height in the updraft-limited regime. The unique behavior of spectral broadening in the updraft-limited regime arises from the S_k and its dependence on droplet radius (see Appendix C). In the updraft-limited regime, S_p and S_k are comparable; together with the size dependence of the S_k, larger particles "win" the competition for water vapor between particles with different radius. This new feature does not exist if the dependence of S_k on size is ignored. It is also found that although N_c is constant and determined by that at the level of maximum supersaturation in the aerosol-limited regime as conventionally assumed, it varies nonlinearly with height in the updraft-limited regime (first increases with increasing height, peaks at certain height, and then decreases with further increasing height). Also, the reason of N_c behavior is related to the critical role of S_k, which causes some small particles to evaporate and eventually deactivate into interstitial particles. However, droplet deactivation likely has a minor role in the spectral broadening in the updraft-limited regime, since only up to 0.08% cloud droplets have negative growth rate.

Relative dispersion exhibits a stronger height dependence. At the level of maximum supersaturation, ϵ increases in the aerosol-limited regime but decreases in the updraft-limited regime as N_a increases. However, this contrasting behavior gradually disappears at high altitudes within the examined range of N_a and w, with the specific height of disappearance relying on the regime. At higher level, increasing N_a/w retards the particle growth in the aerosol-limited regime but enhances the particle growth in the updraft-limited regime (Figure 3b). Thus, condensational broadening in updraft-limited regime is enhanced with larger N_a/w and the contrasting behavior disappears. The enhanced particle growth in updraft-limited regime can be explained below: larger N_a/w causes more evident "kinetic mechanism," smaller N_c, and more evaporation of smaller particles. Thus, larger fraction of large droplets, which are better at water vapor consuming and grow faster in updraft-limited regime, leads to the enhancement of particle growth in the updraft-limited regime.

The regime dependence of rain initiation height is examined by coupling the autoconversion threshold function derived in Liu et al. (2006) with the parcel model simulations. Distinct regime patterns illustrate that the height of rain initiation largely depends on N_a when N_a is small and on w when N_a is large. Cloud microphysical parameters show significant variations and clear regime patterns at the onset of precipitation when the different combinations of N_a and w are considered. This feature suggests that simple parameterizations based on one cloud microphysical properties (e.g., LWC or nth moment mean radius) may cause large errors when there are large variations of N_a and w in the atmosphere. A new expression is proposed to quantify the dependence of H_{rain} on N_a and w.

Two points are noteworthy. First, the results are based on the simulations with fixed typical initial aerosol size distribution parameters, temperature, and relative humidity. The sensitivities to the input aerosol size distributions have been examined, and the main conclusions remain valid, with some subtle differences (see the supporting information for details). The impacts of the initial relative humidity and air temperature are found to be even weaker (see the supporting information for details). Effect of particle hygroscopicity or chemical composition should be examined as well to explore the complete variable space in the ACI regime studies. Second, this study is based on an adiabatic parcel that ignores turbulent entrainment-mixing and collision

coalescence processes. An unresolved question is how the regime patterns (especially for ϵ) will change when these processes are considered. These will be the subject of future study.

Appendix A: Key Model Equations and Further Analysis

Briefly, the cloud parcel model consists of the following key equations. The condensational growth is described by

$$\frac{dm_i}{dt} = 4\pi r_i G \cdot \left(S_p - S_{k,i}\right) \tag{A1a}$$

$$G = \left[\frac{RT}{M_w D'_v e_s} + \frac{l_v}{M_w k'_T T}\left(\frac{l_v}{RT} - 1\right)\left(1 + S_{k,i}\right)\right]^{-1} \tag{A1b}$$

where m is the particle mass, R is the gas constant, D_v' is the diffusion coefficient corrected with molecular kinetics, k_T' is the thermal coefficient corrected with molecular kinetics, e_s is the saturation water vapor pressure, l_v is the latent heat, and subscript "i" represents the ith Lagrangian particle size bin. More details about this equation are in Lamb and Verlinde (2011). The particle radius in each bin is calculated from the particle mass given by

$$r_i = \left(\frac{3}{4}\frac{m_i}{\pi\,\rho_{s,i}}\right)^{\frac{1}{3}} \tag{A2}$$

where ρ_s is the density of the solution. Liquid water mixing ratio q_l, water vapor mixing ratio q_v, air temperature, and air pressure are described by the following equations:

$$\frac{dq_l}{dt} = \frac{1}{\rho_d}\sum_i n_i \frac{dm_i}{dt} \tag{A3}$$

$$\frac{dq_v}{dt} = -\frac{dq_l}{dt} \tag{A4}$$

$$\frac{dT}{dt} = -\frac{gw}{c_p} + \frac{l_v}{c_p}\frac{dq_l}{dt} \tag{A5}$$

$$\frac{dP}{dt} = -\frac{Pgw}{R_a T} \tag{A6}$$

where ρ_d is dry air density, n_i is number concentration per volume air in the ith particle bin, g is gravity acceleration, c_p is air heat capacity, and R_a is gas constant for air. Calculation of S_p is based on T and q_v.

In the simulations presented in the main paper, the initial T, P, and RH are set to be 283.15 K, 919 hPa, and 0.95, respectively. The initial aerosol size distribution is assumed to follow lognormal distribution given by

$$\frac{dn_i}{dr} = \frac{N_a}{\sqrt{2\pi}\,r_i\,\ln\sigma_g}\exp\frac{\left(\ln r_i - \ln r_g\right)^2}{2\ln^2\sigma_g} \tag{A7}$$

where the geometric mean radius r_g is set to be 0.06 μm, the geometric standard deviation σ_g is set to be 1.5.

Appendix B: Maximum Parcel Supersaturation

The parcel supersaturation can be described by

$$\frac{dS_p}{dt} = a\,w - b\frac{d\rho_l}{dt} \tag{A8a}$$

$$a = \left(\frac{gl_v}{c_p R_w T^2} - \frac{g}{R_d T}\right) \tag{A8b}$$

$$b = \frac{R_w T}{e_s} + \frac{R_d l_v^2}{c_p R_w P T} \tag{A8c}$$

where ρ_l is the liquid water density and R_d is the gas constant for dry air. The first term on the right-hand side describes the updraft cooling and is the source term of supersaturation whereas the second term describes condensation-induced depletion of water vapor and is the sink term of supersaturation. As the parcel rises,

the source term dominates first and thus S_p increases with height. At the height of maximum supersaturation, the source and sink terms of the S_p are balanced with each other. Beyond the maximum supersaturation, S_p starts to decrease with further increasing height.

Appendix C: Role of Particle Equilibrium Supersaturation in Condensational Broadening

The condensational narrowing in the aerosol-limited regime has been abundantly studied in the published literature and textbooks (e.g., Pruppacher & Klett, 1997); however, the condensational broadening in the updraft-limited regime has not received much attention because both S_k and its size dependence are usually assumed to be small and ignored. This assumption is incorrect for the updraft-limited regime. We can further understand this by analyzing the expressions for S_k and its variation with radius:

$$S_k = \frac{a_s}{r} - \frac{\kappa r_d^3}{r^3 - r_d^3} \tag{A9a}$$

$$\frac{dS_k}{dr} = -a_s \frac{1}{r^2} + 3\kappa r_d^3 \frac{1}{r^4} \tag{A9b}$$

$$a_s = \frac{2\sigma_s}{R_v \rho_w T} \tag{A9c}$$

where r_d is the dry particle size and κ is the hygroscopicity of aerosols. In the derivation of equation (A9b) from equation (A9a), $r \gg r_d$ is assumed. Equation (A9b) reveals that dS_k/dr is negative since the second term in equation (A9b) is very small due to $r \gg r_d$. The dependence of radius growth rate on radius is given below (Chen et al., 2016; Korolev, 1995).

$$\frac{d\left(\frac{dr}{dt}\right)}{dr} = -\frac{G}{\rho_s r}\left[\frac{S_p - S_k}{r} + \frac{dS_k}{dr}\right] \tag{A10}$$

In the updraft-limited regime, S_p is small and comparable to S_k. The negative dS_k/dr leads to a positive contribution to $(dr/dt)/dr$, which leads to broadening of particle size distribution.

Acknowledgments
This study is supported by grant 2016YFB02008 of the National Major Research High-Performance Computing Program of China and by the U.S. Department of Energy's Atmospheric System Research (ASR and CMDV) program. The simulation data have been uploaded as the supporting information. Yiran Peng is supported by the National Important Project of the Ministry of Science and Technology in China (Grant number is 2017YFC1501404) and National Natural Science Foundation of China (Grant number is 41605106).

References

Albrecht, B. A. (1989). Aerosols, cloud microphysics, and fractional cloudiness. *Science*, *245*(4923), 1227–1230. https://doi.org/10.1126/science.245.4923.1227

Albrecht, B. A., Fairall, C. W., Thomson, D. W., White, A. B., Snider, J. B., & Schubert, W. H. (1990). Surface-based remote sensing of the observed and the Adiabatic liquid water content of stratocumulus clouds. *Geophysical Research Letters*, *17*(1), 89–92. https://doi.org/10.1029/GL017i001p00089

Beard, K. V., & Ochs, H. T. (1993). Warm-rain initiation: An overview of microphysical mechanisms. *Journal of Applied Meteorology*, *32*(4), 608–625. https://doi.org/10.1175/1520-0450(1993)032%3C0608:WRIAOO%3E2.0.CO;2

Berg, L. K., Berkowitz, C. M., Barnard, J. C., Senum, G., & Springston, S. R. (2011). Observations of the first aerosol indirect effect in shallow cumuli. *Geophysical Research Letters*, *38*, L03811. https://doi.org/10.1029/2010GL046047

Cecchini, M. A., Machado, L. A. T., Andreae, M. O., Martin, S. T., Albrecht, R. I., Artaxo, P., … Wendisch, M. (2017). Sensitivities of Amazonian clouds to aerosols and updraft speed. *Atmospheric Chemistry and Physics*, *17*(16), 10037–10050. https://doi.org/10.5194/acp-17-10037-2017

Çelik, F., & Marwitz, J. D. (1999). Droplet spectra broadening by ripening process. Part I: Roles of curvature and salinity of cloud droplets. *Journal of the Atmospheric Sciences*, *56*(17), 3091–3105. https://doi.org/10.1175/1520-0469(1999)056%3C3091:DSBBRP%3E2.0.CO;2

Chen, J., Liu, Y., Zhang, M., & Peng, Y. (2016). New understanding and quantification of the regime dependence of aerosol-cloud interaction for studying aerosol indirect effects. *Geophysical Research Letters*, *43*(4), 1780–1787. https://doi.org/10.1002/2016GL067683

Chen, Y. C., Christensen, M. W., Xue, L., Sorooshian, A., Stephens, G. L., Rasmussen, R. M., & Seinfeld, J. H. (2012). Occurrence of lower cloud albedo in ship tracks. *Atmospheric Chemistry and Physics*, *12*(17), 8223–8235. https://doi.org/10.5194/acp-12-8223-2012

Ching, J., Riemer, N., & West, M. (2012). Impacts of black carbon mixing state on black carbon nucleation scavenging: Insights from a particle-resolved model. *Journal of Geophysical Research*, *117*, D23209. https://doi.org/10.1029/2012JD018269

Ching, J., Riemer, N., & West, M. (2016). Black carbon mixing state impacts on cloud microphysical properties: Effects of aerosol plume and environmental conditions. *Journal of Geophysical Research: Atmospheres*, *121*, 5990–6013. https://doi.org/10.1002/2016JD024851

Christensen, M. W., & Stephens, G. L. (2011). Microphysical and macrophysical responses of marine stratocumulus polluted by underlying ships: Evidence of cloud deepening. *Journal of Geophysical Research*, *116*, D03201. https://doi.org/10.1029/2010JD014638

Chuang, P. Y., Charlson, R. J., & Seinfeld, J. H. (1997). Kinetic limitations on droplet formation in clouds. *Nature*, *390*(6660), 594–596.

Crawford, I., Bower, K. N., Choularton, T. W., Dearden, C., Crosier, J., Westbrook, C., … Blyth, A. (2012). Ice formation and development in aged, wintertime cumulus over the UK: observations and modeling. *Atmospheric Chemistry and Physics*, *12*(11), 4963–4985. https://doi.org/10.5194/acp-12-4963-2012

Feingold, G., Kreidenweis, S. M., Stevens, B., & Cotton, W. R. (1996). Numerical simulations of stratocumulus processing of cloud condensation nuclei through collision-coalescence. *Journal of Geophysical Research*, *101*(D16), 21,391–21,402. https://doi.org/10.1029/96JD01552

Feingold, G., Remer, L. A., Ramaprasad, J., & Kaufman, Y. J. (2001). Analysis of smoke impact on clouds in Brazilian biomass burning regions: An extension of Twomey's approach. *Journal of Geophysical Research*, *106*(D19), 22,907–22,922. https://doi.org/10.1029/2001JD000732

Freud, E., & Rosenfeld, D. (2012). Linear relation between convective cloud drop number concentration and depth for rain initiation. *Journal of Geophysical Research*, *117*, D02207. https://doi.org/10.1029/2011JD016457

Ghan, S. J., Abdul-Razzak, H., Nenes, A., Ming, Y., Liu, X., Ovchinnikov, M., … Shi, X. (2011). Droplet nucleation: Physically-based parameterizations and comparative evaluation. *Journal of Advances in Modeling Earth Systems*, *3*(4), M10001. https://doi.org/10.1029/2011MS000074

Grabowski, W. W., Andrejczuk, M., & Wang, L.-P. (2011). Droplet growth in a bin warm-rain scheme with Twomey CCN activation. *Atmospheric Research*, *99*(2), 290–301. https://doi.org/10.1016/j.atmosres.2010.10.020

Haywood, J., & Boucher, O. (2000). Estimates of the direct and indirect radiative forcing due to tropospheric aerosols: A review. *Reviews of Geophysics*, *38*(4), 513–543. https://doi.org/10.1029/1999RG000078

Heymsfield, A. J., & Sabin, R. M. (1989). Cirrus crystal nucleation by homogeneous freezing of solution droplets. *Journal of the Atmospheric Sciences*, *46*(14), 2252–2264. https://doi.org/10.1175/1520-0469(1989)046%3C2252:CCNBHF%3E2.0.CO;2

Howell, W. E. (1949). The growth of cloud drops in uniformly cooled air. *Journal of Meteorology*, *6*(2), 134–149. https://doi.org/10.1175/1520-0469(1949)006%3C0134:TGOCDI%3E2.0.CO;2

Hudson, J. G., Noble, S., & Jha, V. (2012). Cloud droplet spectral width relationship to CCN spectra and vertical velocity. *Journal of Geophysical Research*, *117*, D11211. https://doi.org/10.1029/2012JD017546

Intergovernmental Panel on Climate Change (2013). *Climate change 2013: The physical science basis. Contribution of Working Group I to the Fifth Assessment Report of the Intergovernmental Panel on Climate Change* (p. 1535). Cambridge, United Kingdom and New York: Cambridge University Press. https://doi.org/10.1017/CBO9781107415324

Korolev, A. V. (1995). The influence of supersaturation fluctuations on droplet size spectra formation. *Journal of the Atmospheric Sciences*, *52*(20), 3620–3634. https://doi.org/10.1175/1520-0469(1995)052%3C3620:TIOSFO%3E2.0.CO;2

Kumar, V. A., Pandithurai, G., Leena, P. P., Dani, K. K., Murugavel, P., Sonbawne, S. M., … Maheskumar, R. S. (2016). Investigation of aerosol indirect effects on monsoon clouds using ground-based measurements over a high-altitude site in Western Ghats. *Atmospheric Chemistry and Physics*, *16*(13), 8423–8430. https://doi.org/10.5194/acp-16-8423-2016

Lamb, D., & Verlinde, J. (2011). *Physics and chemistry of clouds*. New York: Cambridge University Press.

Leaitch, W. R., Strapp, J. W., Isaac, G. A., & Hudson, J. G. (1986). Cloud droplet nucleation and cloud scavenging of aerosol sulfate in polluted atmospheres. *Tellus B*, *38*(5). https://doi.org/10.3402/tellusb.v38i5.15141

Li, Z., Niu, F., Fan, J., Liu, Y., Rosenfeld, D., & Ding, Y. (2011). Long-term impacts of aerosols on the vertical development of clouds and precipitation. *Nature Geoscience*, *4*(12), 888–894. https://doi.org/10.1038/ngeo1313

Li, Z., Xue, H., & Yang, F. (2013). A modeling study of ice formation affected by aerosols. *Journal of Geophysical Research: Atmospheres*, *118*, 11,213–211,227. https://doi.org/10.1002/jgrd.50861

Liou, K. N., & Ou, S. C. (1989). The role of cloud microphysical processes in climate - An assessment from a one-dimensional perspective. *Journal of Geophysical Research*, *94*(D6), 8599–8607. https://doi.org/10.1029/JD094iD06p08599

Liu, Y., & Daum, P. H. (2002). Anthropogenic aerosols: Indirect warming effect from dispersion forcing. *Nature*, *419*(6907). https://doi.org/10.1038/419580a

Liu, Y., Daum, P. H., & McGraw, R. (2004). An analytical expression for predicting the critical radius in the autoconversion parameterization. *Geophysical Research Letters*, *31*, L06121. https://doi.org/10.1029/2003GL019117

Liu, Y., Daum, P. H., McGraw, R., & Miller, M. (2006). Generalized threshold function accounting for effect of relative dispersion on threshold behavior of autoconversion process. *Geophysical Research Letters*, *33*, L11804. https://doi.org/10.1029/2005GL025500

Liu, Y., Daum, P. H., & McGraw, R. L. (2005). Size truncation effect, threshold behavior, and a new type of autoconversion parameterization. *Geophysical Research Letters*, *32*, L03807. https://doi.org/10.1029/2005GL022636

Liu, Y., Daum, P. H., & Yum, S. S. (2006). Analytical expression for the relative dispersion of the cloud droplet size distribution. *Geophysical Research Letters*, *33*, L02810. https://doi.org/10.1029/2005GL024052

Liu, Y., Geerts, B., Miller, M., Daum, P., & McGraw, R. (2008). Threshold radar reflectivity for drizzling clouds. *Geophysical Research Letters*, *35*, L03807. https://doi.org/10.1029/2007GL031201

Lohmann, U., & Feichter, J. (2005). Global indirect aerosol effects: A review. *Atmospheric Chemistry and Physics*, *5*(3), 715–737. https://doi.org/10.5194/acp-5-715-2005

Lohmann, U., & Lesins, G. (2002). Stronger constraints on the anthropogenic indirect aerosol effect. *Science*, *298*(5595), 1012–1015. https://doi.org/10.1126/science.1075405

Lu, C., Liu, Y., Niu, S., & Vogelmann, A. M. (2012). Observed impacts of vertical velocity on cloud microphysics and implications for aerosol indirect effects. *Geophysical Research Letters*, *39*, L21808. https://doi.org/10.1029/2012GL053599

Lu, M.-L., Conant, W. C., Jonsson, H. H., Varutbangkul, V., Flagan, R. C., & Seinfeld, J. H. (2007). The Marine Stratus/Stratocumulus Experiment (MASE): Aerosol-cloud relationships in marine stratocumulus. *Journal of Geophysical Research*, *112*, D10209. https://doi.org/10.1029/2006JD007985

Ma, J., Chen, Y., Wang, W., Yan, P., Liu, H., Yang, S., … Lelieveld, J. (2010). Strong air pollution causes widespread haze-clouds over China. *Journal of Geophysical Research*, *115*, D18204. https://doi.org/10.1029/2009JD013065

Magaritz-Ronen, L., Pinsky, M., & Khain, A. (2016). Drizzle formation in stratocumulus clouds: effects of turbulent mixing. *Atmospheric Chemistry and Physics*, *16*(3), 1849–1862. https://doi.org/10.5194/acp-16-1849-2016

Martins, J. A., & Dias, M. A. F. S. (2009). The impact of smoke from forest fires on the spectral dispersion of cloud droplet size distributions in the Amazonian region. *Environmental Research Letters*, *4*(1), 015002. https://doi.org/10.1088/1748-9326/4/1/015002

Nenes, A., Ghan, S., Abdul-Razzak, H., Chuang, P. Y., & Seinfeld, J. H. (2001). Kinetic limitations on cloud droplet formation and impact on cloud albedo. *Tellus B*, *53*(2), 133–149. https://doi.org/10.1034/j.1600-0889.2001.d01%E2%80%9312.x

Pandithurai, G., Dipu, S., Prabha, T. V., Maheskumar, R. S., Kulkarni, J. R., & Goswami, B. N. (2012). Aerosol effect on droplet spectral dispersion in warm continental cumuli. *Journal of Geophysical Research*, *117*, D16202. https://doi.org/10.1029/2011JD016532

Pawlowska, H., Grabowski, W. W., & Brenguier, J. L. (2006). Observations of the width of cloud droplet spectra in stratocumulus. *Geophysical Research Letters*, *33*, L19810. https://doi.org/10.1029/2006GL026841

Peng, Y., & Lohmann, U. (2003). Sensitivity study of the spectral dispersion of the cloud droplet size distribution on the indirect aerosol effect. *Geophysical Research Letters*, *30*(10), 1507. https://doi.org/10.1029/2003GL017192

Peng, Y., Lohmann, U., Leaitch, R., & Kulmala, M. (2007). An investigation into the aerosol dispersion effect through the activation process in marine stratus clouds. *Journal of Geophysical Research*, *112*, D11117. https://doi.org/10.1029/2006JD007401

Penner, J. E., Quaas, J., Storelvmo, T., Takemura, T., Boucher, O., Guo, H., … Seland, Ø. (2006). Model intercomparison of indirect aerosol effects. *Atmospheric Chemistry and Physics*, *6*(11), 3391–3405. https://doi.org/10.5194/acp-6-3391-2006

Petters, M. D., & Kreidenweis, S. M. (2007). A single parameter representation of hygroscopic growth and cloud condensation nucleus activity. *Atmospheric Chemistry and Physics*, *7*(8), 1961–1971. https://doi.org/10.5194/acp-7-1961-2007

Pincus, R., & Baker, M. B. (1994). Effect of precipitation on the albedo susceptibility of clouds in the marine boundary layer. *Nature*, *372*(6503), 250–252.

Pruppacher, H. R., & Klett, J. D. (1997). *Microphysics of clouds and precipitation, second revised and enlarged edition with an introduction to cloud chemistry and cloud electricity*. Dordrecht, Netherlands: Kluwer Academic Publishers.

Reutter, P., Su, H., Trentmann, J., Simmel, M., Rose, D., Gunthe, S. S., … Pöschl, U. (2009). Aerosol- and updraft-limited regimes of cloud droplet formation: influence of particle number, size and hygroscopicity on the activation of cloud condensation nuclei (CCN). *Atmospheric Chemistry and Physics*, *9*(18), 7067–7080. https://doi.org/10.5194/acp-9-7067-2009

Rotstayn, L. D., & Liu, Y. (2003). Sensitivity of the first indirect aerosol effect to an increase of cloud droplet spectral dispersion with droplet number concentration. *Journal of Climate*, *16*(21), 3476–3481. https://doi.org/10.1175/1520-0442(2003)016%3C3476:SOTFIA%3E2.0.CO;2

Rotstayn, L. D., & Liu, Y. (2009). Cloud droplet spectral dispersion and the indirect aerosol effect: Comparison of two treatments in a GCM. *Geophysical Research Letters*, *36*, L10801. https://doi.org/10.1029/2009GL038216

Ruckstuhl, C., Norris, J. R., & Philipona, R. (2010). Is there evidence for an aerosol indirect effect during the recent aerosol optical depth decline in Europe? *Journal of Geophysical Research*, *115*, D04204. https://doi.org/10.1029/2009JD012867

Segrin, M. S., Jr, J. A. C., & Tahnk, W. R. (2007). MODIS observations of ship tracks in summertime stratus off the West Coast of the United States. *Journal of the Atmospheric Sciences*, *64*(12), 4330–4345. https://doi.org/10.1175/2007jas2308.1

Twomey, S. (1974). Pollution and the planetary albedo. *Atmospheric Environment (1967)*, *8*(12), 1251–1256. https://doi.org/10.1016/0004-6981(74)90004-3

Twomey, S. (1977). The influence of pollution on the shortwave albedo of clouds. *Journal of the Atmospheric Sciences*, *34*(7), 1149–1152. https://doi.org/10.1175/1520-0469(1977)034%3C1149:TIOPOT%3E2.0.CO;2

Wang, L.-P., & Grabowski, W. W. (2009). The role of air turbulence in warm rain initiation. *Atmospheric Science Letters*, *10*(1), 1–8. https://doi.org/10.1002/asl.210

Whitby, K. T. (1978). The physical characteristics of sulfur aerosols. *Atmospheric Environment (1967)*, *12*(1–3), 135–159. https://doi.org/10.1016/0004-6981(78)90196-8

Wood, R. (2006). Rate of loss of cloud droplets by coalescence in warm clouds. *Journal of Geophysical Research*, *111*, D21205. https://doi.org/10.1029/2006JD007553

Wood, R. (2007). Cancellation of aerosol indirect effects in marine stratocumulus through cloud thinning. *Journal of the Atmospheric Sciences*, *64*(7), 2657–2669. https://doi.org/10.1175/JAS3942.1

Wood, R., Irons, S., & Jonas, P. R. (2002). How important is the spectral ripening effect in stratiform boundary layer clouds? Studies using simple trajectory analysis. *Journal of the Atmospheric Sciences*, *59*(18), 2681–2693. https://doi.org/10.1175/1520%26hyphen%3B0469(2002)059%26lt%3B2681:HIITSR%26gt%3B2.0.CO;2

Yuan, T., Remer, L. A., & Yu, H. (2011). Microphysical, macrophysical and radiative signatures of volcanic aerosols in trade wind cumulus observed by the A-Train. *Atmospheric Chemistry and Physics*, *11*(14), 7119–7132. https://doi.org/10.5194/acp-11-7119-2011

Yum, S. S., & Hudson, J. G. (2005). Adiabatic predictions and observations of cloud droplet spectral broadness. *Atmospheric Research*, *73*(3–4), 203–223. https://doi.org/10.1016/j.atmosres.2004.10.006